Assessment of the Fluid Dynamics Boundary Condition in Ablating or Blowing Flows

Brett A. Cruden[1], Dinesh K. Prabhu[1], Arnaud Borner[2], Jeremie Meurisse[2], John Thornton[3], Georgios Bellas-Chatzigeorgis[3]
AMA Inc at NASA Ames Research Center, Moffett Field, CA, 94035

Improved models of ablative thermal protection systems have enabled the treatment of materials and fluid behavior in a coupled manner. This paper reports a new approach to modeling the interface between fluid and material, with attention to the conservation of species mass flux and energy on the fluid side of the interface. The general equation is presented and is shown to recover the traditional uncoupled fluid/materials response interface. Including the chemical reaction terms on the CFD side of the interface makes the heat flux exchange independent of the thermodynamic reference state and, therefore, a measurable quantity. Doing so allows the material response solver to take as input the surface heat flux rather than a film coefficient. Removing the film coefficient approximation enables more direct solution of vehicle thermal response but requires consistency in the wall state. The mixing of the shock layer and pyrolysis gas is then computed with finite rate chemistry within the fluid solver. The boundary conditions described have been implemented in the DPLR v4.05.1 code. Char removal is captured using finite rate chemistry in DPLR's gas surface interaction module. Aspects of coupling these solutions to material response are discussed.

Nomenclature

$\dot{a}_k^{g,c}$	=	atom mass flux (kg/m^2·s)
C_H	=	heat transfer coefficient (kg/m^2·s)
C_M	=	mass transfer coefficient (kg/m^2·s)
G	=	Gibbs free energy (J/kg)
h	=	specific enthalpy (J/kg)
Δh_j	=	heat of reaction *j* (J/kg)
J_s	=	diffusive flux of species *s* (kg/m^2·s)
$\dot{m}$	=	mass flux (kg/m^2·s)
m_s	=	molar mass of species *s* (kg/mol)
n_a	=	number of atoms
n_s	=	number of species
P	=	pressure or partial pressure (Pa)
q	=	heat flux (W/m^2)
r_s	=	surface catalytic mass reaction rate (kg/m^2·s)
R	=	universal gas constant (J/mol·K)
T	=	temperature (K)
$\vec{u}$	=	velocity vector (m/s)
v	=	velocity normal to surface (m/s)
w_s	=	mass fraction of species *s*
x	=	direction normal to interface (m)
z_k	=	mass fraction of atom *k* at wall
α	=	absorptivity
ϵ	=	emissivity
Γ_s	=	kinetic gas flux (kg/m^2·s)
γ_j	=	sticking or reaction coefficient
κ	=	thermal conductivity (W/m·K)
μ	=	viscosity (kg/m^2·s)
υ_{sk}	=	fraction of atom *k* in species *s*
ρ	=	density (kg/m^3)
σ	=	Stefan-Maxwell constant (W/m^2·K^4)
$\chi_k^{g,c}$	=	mass fraction of atom *k*
$\dot{\omega}_{j,s}$	=	mass rate of species s from reaction j

Superscript

-	=	to solid phase
+	=	from gas phase
c	=	char
e	=	edge property
g	=	pyrolysis gas

[1] Sr. Research Scientist, Aerothermodynamics Branch, and AIAA Associate Fellow.
[2] Sr. Research Scientist, Thermal Protection Materials Branch, and AIAA Member.
[3] Research Scientist, Thermal Protection Materials Branch, and AIAA Member.

f = freestream

Subscripts

0 = reference state
a = absorption
c = char or conducted
chem = chemical
d = desorption
e = energy flux (reference state dependent) or boundary layer edge property
eq = equilibrium
f = forward
g = pyrolysis gas
h = heat flux (reference state independent)
j = reaction index
k = atom index
ox = oxidation
r = radiation (incident)
rad = radiation (total)
s = species index
t = condensed phase species index
v = viscous
vap = vaporization
w = wall

I. Introduction

Ablating materials are used in thermal protection systems for atmospheric entry at hypersonic speeds. The performance of an ablating material is studied using a combination of computational fluid dynamics (CFD) and material response models. These models are usually employed in an uncoupled manner, whereby the CFD solution is obtained independently of the material response code. The CFD results are taken as inputs to the material response solver, in which assumptions are made that allow a heating solution to be obtained without requiring the feedback of information such as blowing rates and surface temperature to update the CFD result. In a loosely coupled approach, this information is fed back to the CFD solver, where the simulation is run with a blowing boundary condition.

A variety of coupling approaches have been presented over the past several years. Thompson and Gnoffo in 2008 presented a work to couple the Langley Aerothermodynamic Upwind Relaxation Algorithm (LAURA) code to the Fully Implicit Ablation and Thermal Response (FIAT) code using a modified Stanton number with equilibrium wall compositions [1]. Chen, Milos and Gokcen demonstrated coupled CFD and Material response with the Data Parallel Line Relaxation (DPLR) and FIAT codes in 2010 with equilibrium wall boundary condition and film transfer coefficient exchange of fluxes [2]. Johnston in 2013 applied the equilibrium wall with a 1D material response boundary condition within the LAURA solver, allowing the mass flux conservation to be solved without a film coefficient approximation [3]. In 2014 the work was extended to include finite rate surface reactions [4]. Also in 2014, Chen's approach was extended to solve directly the mass flux equations and to employ the Gas Surface Interaction (GSI) module of MacLean, et al. [5] to include finite rate surface reactions in the CFD model [6]. More recently, Zibitsker, et al. demonstrated a coupling of the CHAMPS solver to a 1D material response to solve the mass and energy balance [7]. Cooper and Martin proposed using the GSI module to compute the char flux in the fluid solver [8]. Schroeder, et al. demonstrated a coupling of the US3D and ICARUS codes through API interactions [9].

Early publications from the GSI module displayed a discrepancy between simulated and experimental heat fluxes on blowing surfaces that was not adequately explained [10]. It is apparent on examination that the heat flux relationship applied in that work and many CFD solvers is not independent of the thermodynamic reference state. While this dependency will drop out in the surface energy balance employed in most materials solvers, it does not provide the physical heat flux on the surface. Furthermore, the film coefficient approximation will embed the reference state in a manner that does not cancel and may become problematic when the blowing gas and shock layer consist of species that cannot be related through reaction mechanisms. As an example, if H_2 is mixing with CO_2, the species have enthalpies of 0.0 and -393.5 kJ/mol at 298.15K in the standard reference state. The aforementioned heat flux relationship would imply that the H_2 is heating the CO_2 gas, which is impossible when they are at the same temperature. The solution to this issue is to formulate the heat flux in a way that is independent of the reference state. This work discusses such a formulation which yields the physical heat flux on the surface by taking much of the surface energy balance into the fluid solver. The formulation accounts for pyrolysis gas blowing from an external material solver, finite rate surface catalysis and finite rate surface char removal and blowing. This boundary condition has been implemented as an option in the DPLR code and used to couple DPLR to the PATO material response solver as reported by Thornton, et al. [11] but could be employed by other material solvers using a simple convective heat flux boundary condition. Additionally, the modification has corrected a long-standing deficiency in simple blowing wall heat flux computations with the DPLR code.

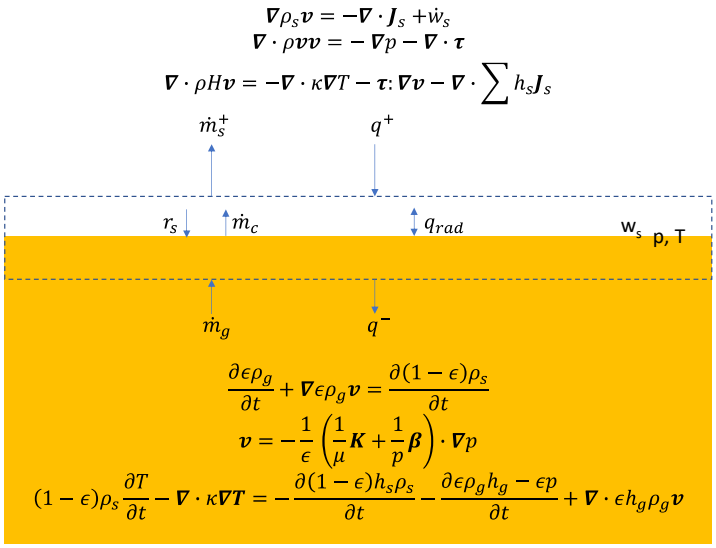

Figure 1. Schematic of the blowing boundary at the fluid material interface, depicted by the dashed region. Fluid and material regions are shown above and below the interface, respectively.

II. Theory

A schematic of a generalized interface between a material and fluid is shown as the dashed region in Figure 1. The fluid and bulk materials are governed by well-known conservation equations above and below the dashed region, respectively. State variables shown (pressure, temperature, mass fractions) maintain the same value across the interface. The difference in fluxes on opposite sides of the interface must equal rates of consumption and production at the interface. Therefore, the species mass balance across the interface is given by:

$$\dot{m}_s^+ - \dot{m}_g w_s^g = \dot{m}_c w_s^c - r_s \tag{1}$$

where s is the species index, $\dot{m}_s^+$ is the species mass flux in the fluid phase and $\dot{m}_g w_s^g$ is the species mass flux in the solid phase. Surface mediated (i.e. catalytic) reactions are given by r_s, where the sign given is in keeping with the direction depicted in Figure 1. The value of r_s may be positive of negative depending on whether the species is consumed or produced, respectively, at the interface. $\dot{m}_g$ and $\dot{m}_c$ are pyrolysis gas and char mass blowing rates, respectively. The mass fraction of pyrolysis and char species are given by w_s^g and w_s^c. The mass fractions must sum to unity, however, the char blowing process may allow for some w_s^c less than zero (if species are consumed, *e.g.*, by oxidation) or greater than one (if the species includes both char and recycled gas phase product).

The change in energy across the interface gives the energy flux balance:

$$q^+ - q^- = -q_{rad} - h_c\dot{m}_c \tag{2}$$

where q^+ and q^- represent the totality of heat flux across the interface. Note that the enthalpies of the gas phase species are contained within these terms. The catalytic reactions convert chemical energy to thermal energy, which is part of the total flux, so do not alter the net energy balance. Removal of char material, on the other hand, occurs at the interface and is not included in the bulk energy, so must be accounted for. The energy removed is the product of the rate of removal, $\dot{m}_c$, and the enthalpy of the solid (unvaporized) char, h_c. The radiation term is meant to include both absorbed radiation and surface re-radiation, *i.e.*,

$$q_{rad} = \alpha q_r - \epsilon\sigma T_w^4 \tag{3}$$

The mass flux in the fluid phase is given by:

$$\dot{m}_s^+ = -(\rho v w_s + J_s) \tag{4}$$

which includes both convective and diffusive fluxes, in the first and second terms, respectively. Note that the following relationships must hold:

$$\sum w_s = 1$$
$$\sum J_s = 0 \tag{5}$$
$$\sum r_s = 0$$

Which together with (1) and (4) imply:

$$\dot{m} = \sum \dot{m}_s^+ = \dot{m}_g + \dot{m}_c = -\rho v \tag{6}$$

Equations (1), (4), and (6) may be combined to provide the relationship for the different surface flux terms:

$$\dot{m} w_s - J_s + r_s = \dot{m}_g w_s^g + \dot{m}_c w_s^c \tag{7}$$

The energy flux from the fluid is given by:

$$q^+ = -\kappa \frac{\partial T}{\partial x}\Big|^+ + \sum_s h_s(\rho v w_s + J_s) + \tfrac{1}{2}\rho u^2 v + \mu\left[\vec{u}\cdot\left(\frac{\partial \vec{u}}{\partial x} + \vec{\nabla} v\right) - \tfrac{2}{3} v \vec{\nabla}\cdot\vec{u}\right] \tag{8}$$

For convenience, we define variables for the terms that represent the conductive and viscous parts of the heat flux:

$$q_c^+ = -\kappa \frac{\partial T}{\partial x}\Big|^+$$
$$q_v^+ = \mu\left[\vec{u}\cdot\left(\frac{\partial \vec{u}}{\partial x} + \vec{\nabla} v\right) - \tfrac{2}{3} v \vec{\nabla}\cdot\vec{u}\right] + \tfrac{1}{2}\rho u^2 v \tag{9}$$

These relationships are then substituted into equation (8), and equation (4) is used to express the heat transfer equation in terms of the mass flux at the interface:

$$q^+ = q_c^+ - \sum_s h_s \dot{m}_s^+ + q_v^+ \tag{10}$$

The heat transfer in the material is given by:

$$q^- = -\kappa \frac{\partial T}{\partial x}\Big|^- - \sum_s h_s \dot{m}_g w_s^g \tag{11}$$

To simplify notation, we define the conduction heat flux into the material:

$$q_c^- = -\kappa \frac{\partial T}{\partial x}\Big|^-$$

The conservation of energy at the interface (2) is now rewritten as:

$$q_c^+ - \sum_s h_s\left(\dot{m}_s^+ - \dot{m}_g\, w_s^g\right) + q_v^+ + h_c \dot{m}_c + q_{rad} = q_c^- \tag{12}$$

This provides a boundary condition for material thermal response in terms of the conducted heat flux. Equation (1) is substituted for the mass flux to produce a simplified form:

$$q_c^- = q_c^+ + q_v^+ + \sum_s h_s r_s + \dot{m}_c(h_c - \sum_s h_s w_s^c) + \alpha q_r - \epsilon\sigma T_w^4 \tag{13}$$

Note that the enthalpies appearing in equation (13) describe the heats of reaction for surface catalysis and char. Equations (7) and (13) form the basis for further discussion of the solution to the interface equation.

A. Equilibrium Approximation

A common approximation is to assume the interface gas is in chemical equilibrium. The chemical equilibrium composition is readily obtained for a fixed atomic ratio at a given temperature and pressure by finding the minimum Gibbs free energy [12]. This is employed in material response solvers since the atomic ratio of pyrolysis gas is generally better known than the exact composition of pyrolysis products. To solve for the equilibrium composition, the species flux equations are replaced by a weaker requirement – the conservation of atomic flux. For atomic conservation, the blowing rate must reproduce the atom mass flux on both sides of the interface. The blowing flux of atom k is given by:

$$\dot{a}_k^g = \dot{m}_g \chi_k^g = \dot{m}_g \sum \upsilon_{sk} w_s^g$$

$$\dot{a}_k^c = \dot{m}_c \chi_k^c = \dot{m}_c \sum \upsilon_{sk} w_s^c \tag{14}$$

Where $\dot{a}_k^{g,c}$ represents the atomic mass flux for atom k in the pyrolysis or char gas, $\chi_k^{g,c}$ is the pyrolysis or char atomic fraction of atom k, and υ_{sk} is the stoichiometry matrix, or mass fraction of atom k in species s. Performing the summations of (14) over equation (7) gives:

$$\dot{m}_g \chi_k^g + \dot{m}_c \chi_k^c = \sum \upsilon_{sk} (\dot{m} w_s - J_s + r_s) \tag{15}$$

Since summation over stoichiometry converts mass fractions to atom fractions and since reactions conserve atoms, the summation over reaction rates is equal to zero; therefore,

$$\dot{m}_g \chi_k^g + \dot{m}_c \chi_k^c = \dot{m} z_k - \sum \upsilon_{sk} J_s \tag{16}$$

where z_k is the atom fraction at the wall. The first term in this equation, the pyrolysis gas blowing, is obtained by integration of the in-depth material response and is known at the interface. Johnston determined J_s iteratively with the fluid dynamics solver [3]. Alternatively, it can be approximated as discussed in the next section. The above relation contains n_a unknowns and n_a-1 unique equations, where n_a is the number of atoms. The gas phase species composition is found by equilibrium solutions that satisfy the atomic ratios. Equilibrium is determined by:

$$-RT \ln \left(\frac{P_s P_0^{\sum \frac{m_s}{m_k} \upsilon_{sk} - 1}}{\prod_k P_k^{\frac{m_s}{m_k} \upsilon_{sk}}} \right) = G_s - \sum \upsilon_{sk} G_k \tag{17}$$

Where P_0 is the pressure of the reference state (typically 1 bar). This set of equations introduces n_s - n_a equations and n_s unknowns. An additional n_a - 1 equations relate partial pressure to the elemental mass fractions:

$$z_k = \frac{\sum_s m_s \upsilon_{sk} P_s}{\sum_{s,j} m_s \upsilon_{sj} P_s} \tag{18}$$

Finally, the partial pressures must sum to equal the total pressure.

$$P = \sum_s P_s \tag{19}$$

The set of equations (16-19) is still underspecified with one degree of freedom. The additional degree of freedom is constrained by placing the solid char in equilibrium with the gas phase:

$$-RT \ln \left(\frac{P_s}{P_0} \right) = \Delta G_{vap,s} \tag{20}$$

Where s indexes the vapor phase gaseous product of the char (typically C). Because the gas phase is in equilibrium, this relationship applies equally to subliming or oxidizing char. The equations do not imply anything about the

mechanism of char removal. They only define the final equilibrium state, which is independent of the mechanism. The equations (16-20) comprise $n_a + n_s$ equations to solve unknowns $z_{1..n_a-1}$, $P_{1..n_s}$, and $\dot{m}_c$.

The equilibrium approximation alters the surface energy balance in that it has effectively introduced chemical reactions at the interface that drive the mixture to equilibrium. Since the reaction rates required to achieve equilibrium are not specified, equation (7) can be substituted into (13) to obtain a relationship in terms of known fluxes:

$$q_c^- = q_c^+ + q_v^+ + \sum_s h_s\left(-\dot{m}w_s + J_s + \dot{m}_g w_s^g\right) + h_c\dot{m}_c + \alpha q_r - \epsilon\sigma T_w^4 \tag{21}$$

Which is rearranged by help of (6) to obtain:

$$q_c^- = q_c^+ + \sum_s h_s J_s + q_v^+ - \dot{m}_g \sum_s h_s\left(w_s - w_s^g\right) - \dot{m}_c\left(\sum_s h_s w_s - h_c\right) + \alpha q_r - \epsilon\sigma T_w^4 \tag{22}$$

This form of the energy balance is similar to that applied in traditional material response solvers, where the first three terms comprise the fluid heat flux, the next two are the enthalpy flux due to pyrolysis gas and char, and the final two terms are radiation. The additional approximation applied in traditional solvers is the film coefficient approximation, discussed in the next section.

B. Film Coefficient Approximation

In addition to the equilibrium assumption, the traditional approximation to the interface equations for uncoupled flow uses a film coefficient to describe the heat and mass transfer. This is the approach commonly employed in material response solvers such as FIAT [13], CHAR, [14], PATO [15] and Icarus [16]. The film coefficient approximation is used to evaluate the transport from the boundary layer edge to the wall, whose properties can be estimated outside of the CFD solver. Heat and mass flux terms are replaced with proportional film coefficient relations. The energy flux at the boundary is written as:

$$q_e^+ = q_c^+ + \sum_s h_s J_s + q_v^+ = C_H\left(\sum_s h_s(T_e) w_{s,e} - h_s(T_w) w_s\right) \tag{23}$$

where the edge enthalpy has been used as an approximation for the adiabatic enthalpy. In the material solver, C_H is typically modified by a blowing correction, which is not discussed here as it does not otherwise alter the equations presented. The wall and edge mass fractions are, at this point, still unknown to the material solver. The diffusive mass flux is replaced with a film coefficient:

$$J_s = C_M\left(w_{s,e} - w_s\right) \approx C_H\left(w_{s,e} - w_s\right) \tag{24}$$

With this approximation equation (16) may be solved:

$$\dot{m}_g \chi_k^g + \dot{m}_c \chi_k^c = (\dot{m} + C_H) z_k - C_H \chi_k^e \tag{25}$$

The χ_k^e are taken to be the atom fractions of the shocked gas, which is approximately the same as the freestream gas. Similar to the previous section, equation (25) is solved along with equilibrium relationships (17-20) to obtain the wall fractions z_k, P_s , and char flux $\dot{m}_c$. The surface energy balance is now given by:

$$q_c^- = C_H\left(\sum_s h_s(T_e) w_{s,e} - h_s w_s\right) - \dot{m}_g \sum_s h_s\left(w_s - w_s^g\right) - \dot{m}_c\left(\sum_s h_s w_s - h_c\right) + \alpha q_r - \epsilon\sigma T_w^4 \tag{26}$$

Which is the same as (22) except for using the film coefficient approximation for the fluid energy flux. This is the form applied in traditional material response solvers.[17]

III. Results

The intent of this work is to directly use equations (7) and (13) as much as possible without requiring film coefficient or equilibrium assumptions. In doing so, different aspects of the above assumptions are discussed. The work is performed using DPLR code [18]. Modifications to the DPLR surface boundary conditions were required to strictly satisfy the above equations and are available in DPLR 4.05.1.

A. Mass Flux Conservation without Char

In the absence of char blowing, the relationships are simplified as there is no longer a need to iteratively determine equilibrium and char mass flux. The surface mass fraction is found from the mass flux relation (7):

$$w_s = w_s^g + \frac{J_s - r_s}{\dot{m}} \tag{27}$$

The pyrolysis gas species conservation w_s^g may be provided as direct input from the material response code. The common approximation currently made in material response is that the pyrolysis gas is in equilibrium at the interface temperature and pressure with atomic ratios specified by χ_k^g. However, this assumption is not mandated for application of these equations. Whether or not an equilibrium wall is assumed, the atomic ratios at the wall satisfy the rearrangement of equation (16):

$$z_k = \chi_k^g + \frac{1}{\dot{m}} \sum \upsilon_{sk} J_s \tag{28}$$

Finally, the film coefficient approximation yields:

$$z_k = \frac{\dot{m}\chi_k^g + C_H \chi_k^e}{\dot{m} + C_H} \tag{29}$$

B. Heat Flux without Char

Two different forms of the surface energy balance have been discussed above, represented by equations (13) and (22). These forms are shown to be equivalent by substitution of species mass flux balance, equation (7). However, the two forms encourage different formulations of the heat flux. The heat flux employed in the uncoupled problem is suggested by equation (22) and is stated on the left-hand side of equation (23):

$$q_e^+ = q_c^+ + q_v^+ + \sum_s h_s J_s \tag{30}$$

The heat flux suggested by equation (13) is given by:

$$q_h^+ = q_c^+ + q_v^+ + \sum_s h_s r_s = q_c^+ + q_v^+ + \sum_s h_s \left(J_s - \dot{m}\left(w_s - w_s^g \right) \right) \tag{31}$$

Comparison of the second form of (31) to (30) shows that these fluxes differ only by the inclusion of advective terms on both sides of the interface. The uncoupled form of the heat flux (30) is dependent upon the thermodynamic reference state and is therefore not a measurable quantity[1]. While blowing gases are known to impact heat transfer at a surface, the reference state, being arbitrarily defined, cannot introduce a cooling (or heating) effect. Equation (30) is only meaningful when employed in conjunction with the energy balance (22) evaluated using the same reference state. While this is possible through use of conventions or standardized databases, the approach is prone to error when solvers are developed and applied independently. Furthermore, the film coefficient approximation (23) embeds the reference state in C_H, and it is not unambiguously removed in the evaluation of heat flux (26). The form of equation (31), on the other hand, is independent of the thermodynamic reference state (as shown in Appendix A) and is, therefore, a physically meaningful, measurable heat flux. While this discussion thus far has been applied to a pyrolyzing gas flow, the relationships discussed here are applicable to any blowing boundary condition. Thus, the boundary conditions in DPLR have been revised as discussed in the next section.

C. Demonstration without Char

The DPLR code includes four boundary conditions that are designed for coupling to material response with external blowing rates that can be specified at individual surface points. Additionally, there are a series of boundary conditions designed to use the freestream mixture as the blowing gas. These boundary conditions are summarized in Table 1. Boundary conditions in the 30's, 130's, 230's and 300's use the freestream composition for the blowing gas.

[1] Since reference states are arbitrary quantities, they must cancel out in physically meaningful calculations. Quantities that depend on them then do not have a physical meaning in an absolute sense but may be physically significant after further evaluation. To distinguish the physical significance of such a quantity, we refer to the reference state independent value as a "measurable quantity."

The boundary conditions 70 and 71 are intended for the case where the surface mixture is specified, while 72 and 73 specify the blowing (here, pyrolysis) gas injection. The differences between 70 and 71 or 72 and 73 are only in the form of the input variables. The species mass fluxes may be converted to total mass flux and mole fractions or vice versa. Options 70/71, then, are the appropriate boundary conditions to use for a material response solution that employs the film coefficient approximation (with or without equilibrium) to determine the surface species concentrations, while 72/73 are a more general boundary condition requiring only knowledge of pyrolysis gas blowing.

For boundary condition 70/71, the mass fractions at the wall are fixed input, comprising a Dirichlet boundary condition. Since the gas fractions are pre-determined, neither w_s^g nor r_s can be determined by the solver without making some assumptions about the user's intent. Therefore, the reference state dependent equation (30) is employed for the heat flux. It is noted that the 4th term of equation (22), if added to equation (30), would yield the physical heat flux given in equation (31). This computation must then be performed external to DPLR. However, any inconsistency between the fluid J_s and the material solver J_s will not fully cancel the reference state energy.

For BCs 72/73 where only the pyrolysis gas fractions are provided, DPLR can accurately solve the diffusive flux while determining the surface concentration. The boundary condition is then formulated in terms of the mass fluxes, but also depend on the mass fractions, so are described in Table 1 as a Robin boundary condition. More generally, surface reactions may introduce non-linear dependence upon the dependent variables. Thus, the boundary condition requires a linearization of reaction terms and the diffusive flux is formulated using finite differences to represent the gradients, depending upon the diffusion model employed. The resulting matrix equations are solved implicitly along with the rest of the flowfield solution [10]. Finally, the freestream blowing boundary conditions are solved in the same manner as BC 73.

Table 1. Summary of blowing and pyrolysis boundary conditions in DPLR

Description	DPLR BC Number	Inputs	Surface mass fraction	Heat Flux	BC Type
Freestream Gas Blowing	3X, 13X, 23X, 3XX	$\dot{m}, T$	$w_s = w_s^f + \frac{J_s - r_s}{\dot{m}}$	(31)	Mass Flux (Robin)
Mixture Gas Fluxes	70	$\dot{m}_s^+, T$	$w_s = \frac{\dot{m}_s^+}{\sum \dot{m}_s^+}$	(30)	Mass Fraction (Dirichlet)
Mixture Gas Fractions	71	$\dot{m}, w_s, T$	$w_s = w_s$		
Blowing Gas Fluxes	72	$\dot{m}_s^- = \dot{m} w_s^g, T$	$w_s = \frac{\dot{m}_s^- + J_s - r_s}{\sum \dot{m}_s^-}$	(31)	Mass Flux (Robin)
Blowing Gas Fractions	73	$\dot{m}, w_s^g, T$	$w_s = w_s^g + \frac{J_s - r_s}{\dot{m}}$		

The implementation of the boundary conditions is tested using a 1 m radius sphere with freestream at conditions representative of MSL entry conditions just prior to turbulent transition, similar to that discussed in [11]. The freestream condition corresponds to a velocity of 5.52 km/s and density 4.25 x 10^{-4} kg/m^3 (2.91% N_2 in CO_2, by weight). A surface temperature and pyrolysis blowing rate is computed using the PATO code based on an initial non-blowing DPLR solution, as would be used in the uncoupled approach. The pyrolysis gas is computed at each surface point at equilibrium and consists mainly of CH_4, CO and H_2. The surface temperature varies from 750K at the edge to 1550K at the stagnation point with mass fluxes from 3 x 10^{-4} to 8 x 10^{-3} kg/m^2-s. An updated chemistry is implemented to predict the reaction of blowing gas with shock layer gas and given in Appendix B.

Figure 2 shows a comparison of heating rates on the sphere using the same mass flux boundary condition but different heat flux equations. Figure 2(a) shows the heat flux calculated for a blowing, non-catalytic wall. The heat flux obtained with reference state independence (labeled '31') increases by up to 6% over the dependent ('30') quantity. Also shown is the chemical component of the heat flux (third term in equations (30, 31)). For a non-catalytic wall, this contribution is zero when evaluated independently of the reference state but is negative when the reference state energy is included. The fully catalytic wall case in Figure 2(b) shows an even larger increase in heat flux, up to 10%, when evaluated independently from the reference state. The difference is contributed entirely by the chemical term. Figure 2(c) shows the chemical component of the fully catalytic heat flux using different reference states of 0 and 298.15 K. The impact of the reference state on the chemical heat flux for this case is between 1-3% using equation (30) and <0.01% by equation (31), the latter difference being a result of machine error/convergence. It is noted that

the solutions using the two different reference states do not bound the physical chemical heat flux, which is 5-27% larger, so may not be used to estimate the impact of the reference state.

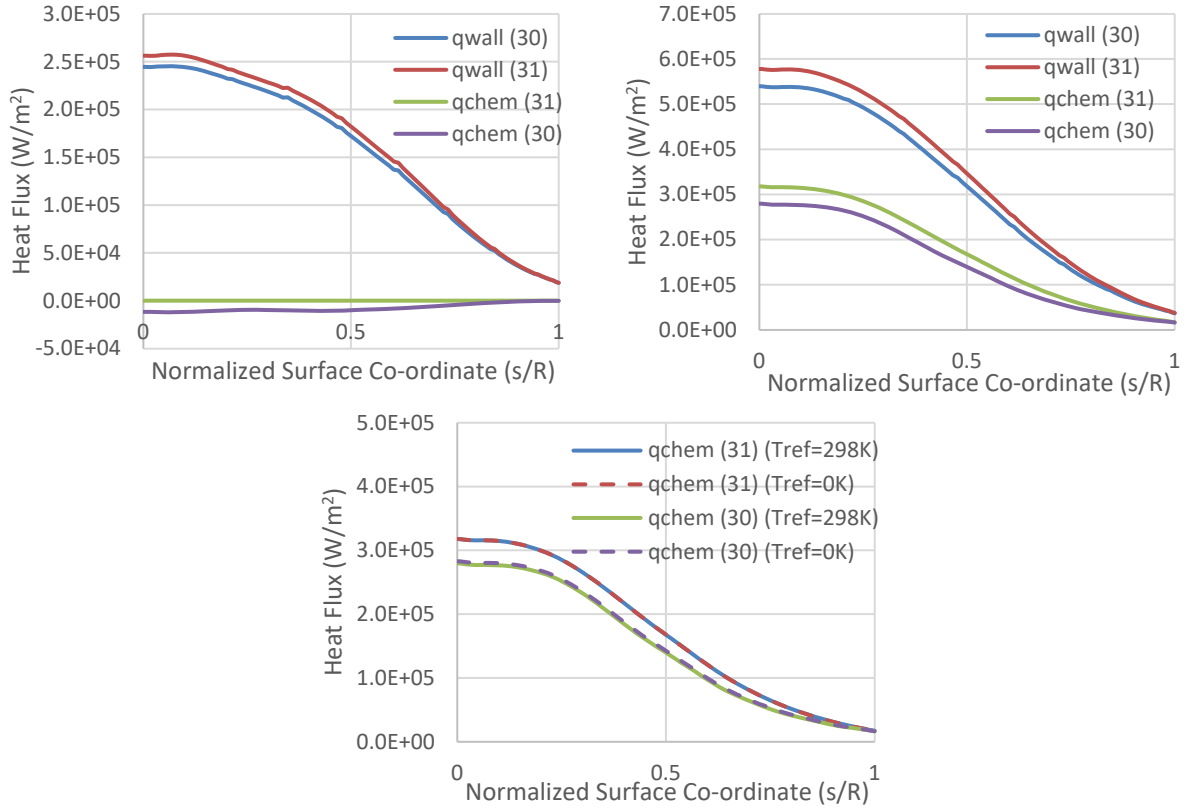

Figure 2. Heat Flux on a blowing unit sphere, with original form of heat flux equation and with reference state independent formulation. Shown are total heat fluxes and the chemical portion of heat flux. (a) Non-catalytic, (b) fully-catalytic, (c) chemical term only with different reference states (fully catalytic)

D. Heat and Mass Transfer including Char Removal

The impact of char removal on the heat and mass balance was discussed in Sect. II, along with the methodology by which char flux is obtained under the equilibrium assumption. Relationships for non-equilibrium or finite rate char removal have been discussed extensively in the literature but are not employed in material or fluid solvers as a matter of course. Many of the existing mechanisms employ irreversible chemical processes, which may be reasonable for many ablating scenarios. However, since the traditional approach is built upon equilibrium assumptions, only mechanisms where all rates are written reversibly will be able to obtain the traditional equilibrium value in the limit. With this in mind, we discuss two important mechanisms of non-equilibrium char removal – sublimation and oxidation. More detailed mechanisms and equations may be found in the existing literature. For both of these mechanisms, the char species flux from the surface is built upon gas kinetic theory. The kinetic flux of species to a surface is given by:

$$\Gamma_s = P_s\sqrt{\frac{m_s}{2\pi RT}} \tag{32}$$

The absorption of the species on the surface may be characterized by a sticking coefficient, γ_j, where j is a reaction, rather than species, index. γ_j must be between 0 and 1. The rate of absorption is therefore given by:

$$r_{a,j} = \gamma_j P_s\sqrt{\frac{m_s}{2\pi RT}} \tag{33}$$

At equilibrium, the rate of desorption equals the rate of absorption:

$$r_{d,j,eq} = \gamma_j P_{s,eq} \sqrt{\frac{m_s}{2\pi RT}} \tag{34}$$

Based on detailed balance, the desorption rate is independent of the gas phase composition, thus the relationship for desorption must also hold in non-equilibrium. The char blowing rate from reaction j now may be computed as the difference between desorption and adsorption:

$$\dot{m}_{c,j} = r_{d,j} - r_{a,j} = \gamma_j \left(P_{s,eq} - P_s\right) \sqrt{\frac{m_s}{2\pi RT}} \tag{35}$$

The equilibrium relationship established in equation (20) is then inserted:

$$\dot{m}_{c,j} = \gamma_j \left(P_0 e^{-\frac{\Delta G_{vap,s}}{RT}} - P_s\right) \sqrt{\frac{m_s}{2\pi RT}} \tag{36}$$

With this relationship, the char blowing rate may be found given the partial pressure of the gas phase char product and a relationship for the sticking coefficient.

The above relationship involves only one gas phase species, thus it represents a sublimation process. One could consider instead an oxidation process, e.g.

$$O(g) + C(s) \leftrightarrow CO(g) \tag{37}$$

In this case, one may replace the sticking coefficient with a reaction probability, γ_{ox} which may itself be a function of temperature:

$$r_{f,\mathrm{ox}} = \gamma_{ox} P_O \sqrt{\frac{m_O}{2\pi RT}} \tag{38}$$

Including the reverse reaction:

$$r_{\mathrm{ox}} = \gamma_{ox} \left(P_O - P_{CO} e^{-\frac{\Delta G_{ox}}{RT}}\right) \sqrt{\frac{m_O}{2\pi RT}} \tag{39}$$

Similar equations can be developed for several variations of surface reactions, including mechanisms that depend upon surface site availability, as in Langmuir-Hinshelwood kinetics. Such a set of equations are already available in DPLR via the Gas Surface Interaction (GSI) module. [5, 19] Similar equations have also been implemented in material response codes, such as FIAT [20] and the LAURA CFD code [4]. For coupled material response, it is only necessary to solve these reactions in one of the two codes (i.e. one side of the interface) and the resulting boundary condition may then be transmitted to the other solver. Since the GSI module is already embedded within DPLR, this approach is taken in this work, with some modifications to be discussed.

The GSI module provides an overall reaction rate at the surface for species entering or leaving the gas phase. Unlike the formulation provided in Sect. II, the net result would not distinguish between reactions involving char or catalysis. To put the results in terms of already established relationships, we write the output as the combination of catalysis and char rates, which in turn is the sum over all reactions considered in the GSI module:

$$r_s - \dot{m}_c w_s^c = \sum_j \dot{\omega}_{j,s} \tag{40}$$

Where $\dot{\omega}_{j,s}$ is the rate of mass production of species s by reaction j. With this relation, it is unnecessary to determine w_s^c explicitly. The rate of char removal is obtained by summing (40) over all the species and applying equation (5):

$$\dot{m}_c = -\sum_{j,s} \dot{\omega}_{j,s} \tag{41}$$

Note that $\dot{\omega}_{j,s}$ does not sum to zero because the solid phase species (i.e. char) are not included in the summation. We may write the summation over these species as:

$$\dot{m}_c = \sum_{j,t\notin s} \dot{\omega}_{j,t} \tag{42}$$

The summation over the solid species is equal and opposite the gas phase species to satisfy mass conservation.

The heat flux attributable to the solid char is found by summing over the mass action on the solid phase:

$$h_c \dot{m}_c = \sum_{j,t\notin s} h_t \dot{\omega}_{j,t} \tag{43}$$

The combined heat flux for char and catalysis can be found by summing over all reactions:

$$q_{chem} = \sum_s h_s (r_s - \dot{m}_c w_s^c) + \dot{m}_c h_c = \sum_{j,s} h_s \dot{\omega}_{j,s} + \sum_{j,t\notin s} h_t \dot{\omega}_{j,t} = \sum_j \Delta h_j \dot{\omega}_j \tag{44}$$

Heats of reaction are required for reversible reactions, so this quantity may be computed directly in the GSI module, using Lewis fits of the solid materials. The modified mass and heat flux balances at the interface may now be written as:

$$\dot{m} w_s - J_s + \sum_j \dot{\omega}_{j,s} = \dot{m}_g w_s^g \tag{45}$$

$$q_c^- = q_c^+ + q_v^+ + \sum_j \Delta h_j \dot{\omega}_j + \alpha q_r - \epsilon \sigma T_w^4 \tag{46}$$

The GSI module required modifications to compute and return the char removal rate, $\dot{m}_c$ and the chemical flux q_{chem} according to the above equations. Additionally, the pyrolysis option within GSI was not used since the pyrolysis gas rate was supplied externally, which also required modifications to DPLR.

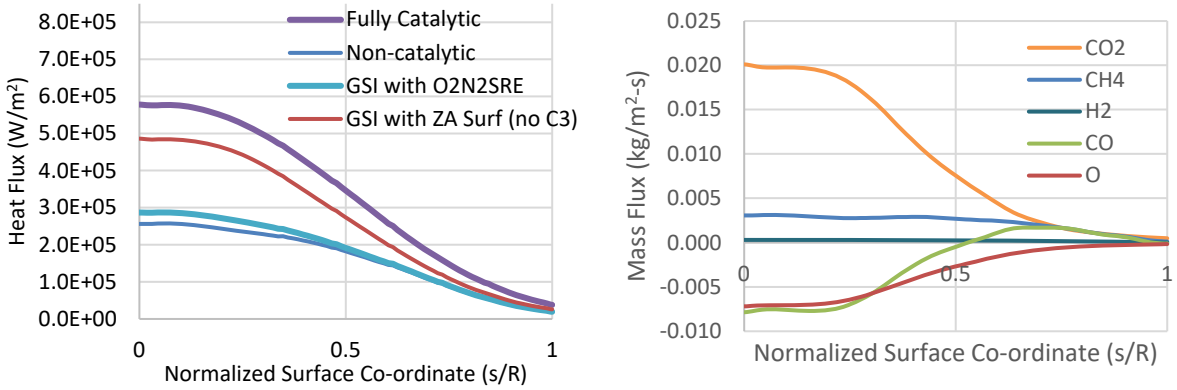

Figure 3. Solutions on blowing unit sphere with carbon char. (a) Heat Flux with different surface models, (b) Mass blowing for pyrolysis and ZA char.

E. Demonstration with Char Removal

A demonstration of the char blowing boundary condition applied to the same case in Section C is shown in Figure 3. Figure 3(a) shows the heat flux computed on the same unit sphere with four different surface models: non-catalytic, fully-catalytic, GSI with surface site balance catalysis, and GSI with the Zhluktov-Abe (ZA) Model [21] with C_3 omitted. For this case, the non-catalytic and fully-catalytic solutions bracket the GSI solutions. The site balance catalysis falls closer to the non-catalytic case, while the ZA surface mechanism is closer to fully catalytic. The reason for the higher heat flux in the ZA model is apparent from Figure 3(b) which shows the species flux in the gas phase. The main blowing species is CO_2 which is produced by a surface mediated reaction between CO and O. These species in turn are both consumed at the surface. Closer to the edge of the sphere, there is a net outward flux of CO due to its production as a pyrolysis gas. CH_4 and H_2 are also blown from the surface as pyrolysis products and do not participate in any surface reactions. The third largest surface reaction in this model is direct sublimation of atomic C, however,

this rate is much lower than O atom adsorption and Eley-Ridel recombination of CO(g) with O(ad). Thus, under these conditions, similar to a Mars 2020 entry, the amount of char removal is relatively small.

A second example shown in Figure 4 uses a contrived Silica char model at a higher surface temperature. The contrived model considers the desorption of non-reacting gaseous SiO from SiO_2 (quartz) bulk with unity sticking probability. The thermodynamic properties of gaseous SiO and solid SiO_2 are based upon Lewis curve fits [12], but the transport properties are assumed identical to other blowing species. The surface temperature is artificially increased by 1000K over the previous example to induce silica vaporization but the pyrolysis gas blowing rate is unchanged. The heat flux in Figure 4(a) is shown with and without the char removal enthalpy (eq. 43). The char removal enthalpy lowers the heat flux near the front of the sphere where sublimation is significant. The plot of the corresponding mass fluxes is shown in Figure 4(b). CO, CO_2, and H_2O are all pyrolysis-blowing species comprising the majority of the mass flux. The decomposition of SiO_2 in this model produces desorbed SiO and O atoms. While the mass desorbed is small, the contribution to the enthalpy is significant due to the energy of dissociation and vaporization. The fluctuations observed in the blowing rates and heat flux with char enthalpy included are due to variations in the imposed temperature profile propagating into the GSI computation.

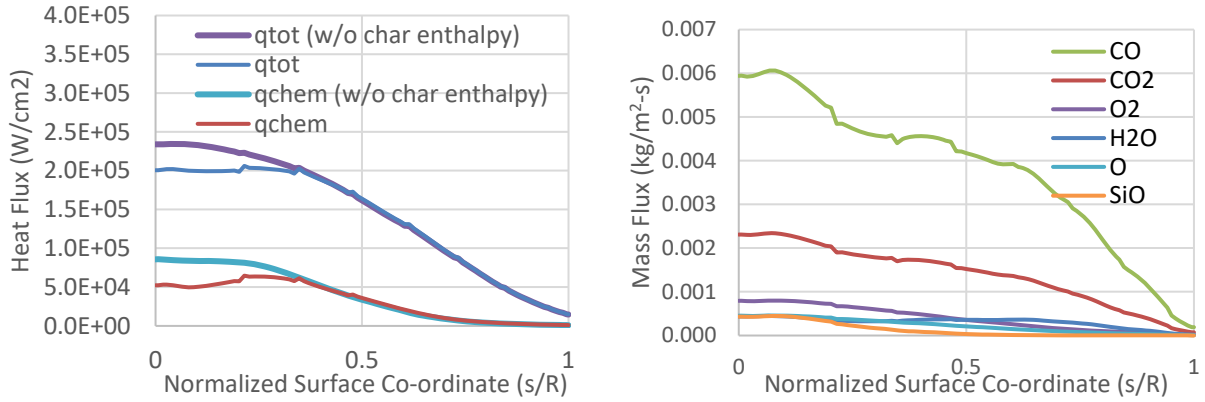

Figure 4. Solutions on a blowing unit sphere with silica char. (a) Heat flux with and without the char removal enthalpy included. The total and chemical component are shown. (b) Mass blowing for contrived silica char model. Fluctuations in cases with char enthalpy are due to non-smoothness in the surface temperature profile.

F. Implications for Material Coupling

The material response coupling with the discussed fluid boundary conditions is shown schematically in Figure 5. With all the surface reactions computed in the GSI module, it is no longer required to solve the entire surface energy balance in the material response code. This uses the heat flux boundary condition that is available in codes such as FIAT and PATO. In this mode, the material response only computes the re-radiation and in-depth conduction terms of the surface energy balance which depend upon the surface temperature obtained. The convective and chemical heat fluxes are evaluated directly by DPLR and GSI, respectively. Table 2 summarizes the parameters passed between solvers and the quantities solved for in terms of mass, momentum, and energy conservation. The mass flux equations are solved in DPLR, with the external blowing rate provided from PATO by species. The blowing gases are balanced by the convective and diffusive fluxes in DPLR and reactive flux (including catalysis and char) from GSI. The wall blowing velocity, density and pressure is determined by the CFD solver given the blowing flux. The pressure, in turn, is used by the material solver to calculate the outgoing flux. Finally, the CFD solver takes a surface temperature as input to compute the wall-directed heat flux. This heat flux is then combined with the radiative heat flux in the material solver to re-compute the conducted heat and surface temperature. Due to differences in time scale, the fluid is typically solved in steady state at relatively large separations in time while the transient material response is evaluated between the fluid time points. These steps may be iterated until all quantities are converged. The surface temperature is probably the most practical (and meaningful) metric for convergence.

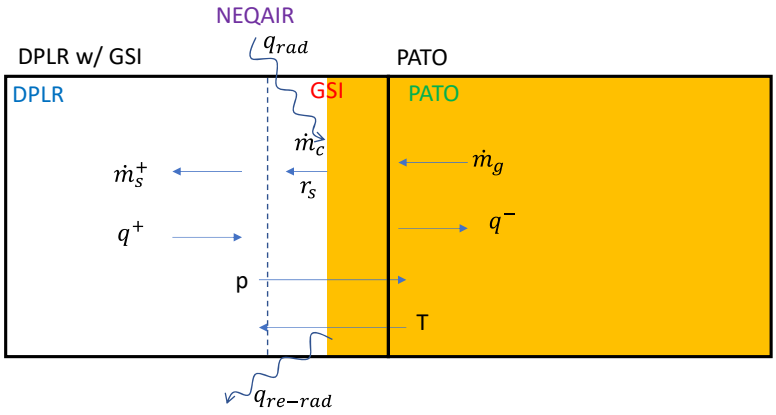

Figure 5. Schematic of proposed material-fluid coupling with DPLR CFD code, PATO material response, NEQAIR radiation, and the GSI interface module.

Table 2. Interface parameters received and returned by each solver for the general coupling problem

	CFD (DPLR)	Material Response (PATO)
Mass/Species	Given $\dot{m}_g w_s^g$, find w_s	Find w_s^g
Momentum	Given $\dot{m}_g$, compute P	Given P, compute $\dot{m}_g$
Energy	Given T, compute q	Given q, compute T

The char mass flux computed by the GSI module will need to be fed back to PATO to compute material recession rates. The film coefficient is no longer required to compute recession, nor is the recession rate required by PATO to compute the energy balance. The only impact of the recession in PATO is to translate the surface grid, which in turn impacts the in-depth temperature profile. A second-order impact of the recession will be to move the surface grid within DPLR, which may be examined in future work.

A final note is added regarding the transfer of data between fluid and material solvers. The computation of a reacting fluid solver generally scales as n_s^2 and requires reaction rates and pairwise transport coefficients for all the species. These requirements tend to limit the number of species within the fluid simulation. The material solver, however, particularly when considering full equilibrium, may include a much larger number of species within the pyrolysis gas. The translation of pyrolysis blowing flux between the solvers then may involve a conversion of species using equilibrium while conserving the atomic ratios. While this is a practical consideration for data exchange, it does alter the energy of the pyrolysis gas and so introduces an additional heat flux term to be included at the surface:

$$q_{intfc} = \dot{m}_g\left(\sum_{i\in PATO} h_i(T) w_i^- - \sum_{s\in DPLR} h_s(T) w_s^g\right) \tag{47}$$

Note that w_i^- represents the in-depth pyrolysis gas mass fractions approaching the surface and may differ from the w_s^g mass fractions that are passed to the fluid solver at the interface. Each set sums to one and derives the same χ_k^g:

$$\sum_{i\in PATO} w_i^- = \sum_{s\in DPLR} w_s^g = 1$$

$$\sum_{i\in PATO} \upsilon_{ik} w_i^- = \sum_{s\in DPLR} \upsilon_{sk} w_s^g = \chi_k^g \tag{48}$$

If the PATO and DPLR sets are equal, there is a one-to-one mapping from i to s with $w_i^- = w_s^g$ and eq (47) goes to zero.

IV. Conclusions

This paper has described a general methodology for computing energy and mass exchange at a blowing interface in a computational fluid dynamics solver. The discussion is made in the context of an ablating (pyrolyzing and/or

charring) flow as is commonly encountered in entry vehicles. General surface interface equations in species mass and energy flux are discussed and it is shown how these reduce to the traditional material response equations assuming chemical equilibrium and film coefficient approximation to uncoupled transport. A modification to the heat flux formulation is recommended in order to remove the reference enthalpy dependence from the quantities passed between codes. Doing so removes the chemical heat flux terms from the material surface energy balance and places them within the fluid solver. This has the benefit of providing a heat flux that is physically measurable and avoids possible inconsistencies in enthalpy calculations between material and CFD solvers due to differences in reference state and/or thermodynamic database. The mass and heat flux equations for a general blowing gas are the same as for the case of pyrolysis without char, and given by equations (27) and (31):

$$w_s = w_s^g + \frac{J_s - r_s}{\dot{m}}$$

$$q_h^+ = q_c^+ + q_v^+ + \sum_s h_s r_s = q_c^+ + q_v^+ + \sum_s h_s \left(J_s - \dot{m}\left(w_s - w_s^g\right)\right)$$

In the presence of char blowing, the catalysis and char reaction/sublimation rates are consolidated into a set of surface reaction terms and the mass and heat fluxes are represented by generalizations of the equations without char:

$$\dot{m} w_s - J_s + \sum\nolimits_j \dot{\omega}_{j,s} = \dot{m}_g w_s^g$$

$$q_h^+ = q_c^+ + q_v^+ + \sum\nolimits_j \Delta h_j \dot{\omega}_j$$

An approach to computing char blowing in the above framework is discussed using the GSI module within DPLR. These results allow heat flux to be passed directly to the material response solver, which then determines the surface temperature and pyrolysis blowing rates. Char removal rate is passed from the GSI to the material solver to advance the surface mesh and impact the temperature profiles. These approaches have been implemented in DPLR v4.05.1 for general blowing and material response boundary conditions. The traditional option of coupling to material response via specified wall mass fractions, which uses a reference state dependent form of the heat flux has also been retained. This method is intended to be used with the traditional film coefficient based surface energy balance. Results of this work are currently in use in PATO/DPLR based coupling simulations of MSL and Mars2020 entries [11], which will be reported further in future publications.

Acknowledgments

Support from the Entry Systems Modeling Project is acknowledged. AMA authors are supported through contract NNA15BB15C to AMA, Inc.

References

1. Thompson, R. A., and Gnoffo, P. A. "Implementation of a Blowing Boundary Condition in the LAURA Code," 2008,
2. Chen, Y.-K., Milos, F. S., and Gokcen, T. "Loosely Coupled Simulation for Two-Dimensional Ablation and Shape Change," *Journal of Spacecraft and Rockets* Vol. 47, No. 5, 2010, pp. 775-785. doi: 10.2514/1.39667
3. Johnston, C. O., Gnoffo, P. A., and Mazaheri, A. "Influence of Coupled Radiation and Ablation on the Aerothermodynamic Environment of Planetary Entry Vehicles," VKI 2013-AVT-218, 2013,
4. Johnston, C. O. "Study of Aerothermodynamic Modeling Issues Relevant to High-Speed Sample Return Vehicles," Vol. STO-AVT-218, VKI 2013-AVT-218, 2014,
5. MacLean, M., Marschall, J., and Driver, D. "Finite-Rate Surface Chemistry Model, II: Coupling to Viscous Navier-Stokes Code," *42nd AIAA Thermophysics Conference*, 2011. doi: 10.2514/6.2011-3784
6. Chen, Y.-K., and Gökçen, T. "Implicit Coupling Approach for Simulation of Charring Carbon Ablators," *Journal of Spacecraft and Rockets* Vol. 51, No. 3, 2014, pp. 779-788. doi: 10.2514/1.A32753
7. Zibitsker, A. L., McQuaid, J., Brehm, C., and Martin, A. "Fully-Coupled Simulation of Low Temperature Ablator and Hypersonic Flow Solver," *AIAA SCITECH 2022 Forum*, 2022. doi: 10.2514/6.2022-0676

8. Cooper, J. M., and Martin, A. "Novel Engineering Methodology for Decoupled Aerothermal Analysis of Hypersonic Atmospheric Entry Flows," *Journal of Spacecraft and Rockets* Vol. 60, No. 2, 2023, pp. 437-453. doi: 10.2514/1.A35433
9. Schroeder, O. M., Brock, J., Stern, E., and Candler, G. V. "A coupled ablation approach using Icarus and US3D," *AIAA Scitech 2021 Forum*, 2021. doi: 10.2514/6.2021-0924
10. MacLean, M., Barnhardt, M., and Wright, M. "Implicit Surface Boundary Conditions for Blowing, Equilibrium Composition, and Diffusion-Limited Oxidation," *48th AIAA Aerospace Sciences Meeting Including the New Horizons Forum and Aerospace Exposition*, 2010. doi: 10.2514/6.2010-1179
11. Thornton, J. M., Prabhu, D. K., Meurisse, J. B., Borner, A., Monk, J. D., and Cruden, B. A. "Coupling Heatshield Response and Aerothermal Environment for Mars Entry via Surface Gas Blowing," *AIAA SCITECH 2023 Forum*, 2023. doi: 10.2514/6.2023-0963
12. Gordon, S., and McBride, B. J. "Computer program for calculation of complex chemical equilibrium compositions and applications I. Analysis," NASA RP-1311, 1994,
13. Milos, F. S., and Chen, Y. K. "Ablation, Thermal Response, and Chemistry Program for Analysis of Thermal Protection Systems," *Journal of Spacecraft and Rockets* Vol. 50, No. 1, 2013, pp. 137-149. doi: 10.2514/1.A32302
14. Amar, A. J., Oliver, B., Kirk, B., Salazar, G., and Droba, J. "Overview of the CHarring Ablator Response (CHAR) Code," *46th AIAA Thermophysics Conference*, 2016. doi: 10.2514/6.2016-3385
15. Meurisse, J. B. E., Lachaud, J., Panerai, F., Tang, C., and Mansour, N. N. "Multidimensional material response simulations of a full-scale tiled ablative heatshield," *Aerospace Science and Technology* Vol. 76, 2018, pp. 497-511. doi: 10.1016/j.ast.2018.01.013
16. Schulz, J. C., Stern, E., Muppidi, S., Palmer, G., Schroeder, O., and Martin, A. "Development of a three-dimensional, unstructured material response design tool," *55th AIAA Aerospace Sciences Meeting*, 2017. doi: 10.2514/6.2017-0667
17. Chen, Y. K., and Milos, F. S. "Two-Dimensional Implicit Thermal Response and Ablation Program for Charring Materials," *Journal of Spacecraft and Rockets* Vol. 38, No. 4, 2001, pp. 473-481. doi: 10.2514/2.3724
18. Wright, M. W., White, T., and Mangini, N. "Data Parallel Line Relaxation (DPLR) Code User Manual Acadia – Version 4.01.1," NASA/TM-2009-215388, 2009,
19. Marschall, J., and MacLean, M. "Finite-Rate Surface Chemistry Model, I: Formulation and Reaction System Examples," *42nd AIAA Thermophysics Conference*, 2011. doi: 10.2514/6.2011-3783
20. Milos, F., Chen, Y.-K., and Gokcen, T. "Non-Equilibrium Ablation of Phenolic Impregnated Carbon Ablator," 2010. doi: 10.2514/6.2010-981
21. Zhluktov, S. V., and Abe, T. "Viscous Shock-Layer Simulation of Airflow past Ablating Blunt Body with Carbon Surface," *Journal of Thermophysics and Heat Transfer* Vol. 13, No. 1, 1999, pp. 50-59. doi: 10.2514/2.6400
22. Gokcen, T. "N2-CH4-Ar Chemical Kinetic Model for Simulations of Atmospheric Entry to Titan," *Journal of Thermophysics and Heat Transfer* Vol. 21, No. 1, 2007, pp. 9-18. doi: 10.2514/1.22095
23. Martin, A., Cozmuta, I., Wright, M. J., and Boyd, I. D. "Kinetic Rates for Gas-Phase Chemistry of Phenolic-Based Carbon Ablator in Atmospheric Air," *Journal of Thermophysics and Heat Transfer* Vol. 29, No. 2, 2015, pp. 222-240. doi: 10.2514/1.T4184
24. Cruden, B. A., Brandis, A. M., and MacDonald, M. E. "Characterization of CO Thermochemistry in Incident Shockwaves," *2018 Joint Thermophysics and Heat Transfer Conference* 2018-3768, 2018. doi: 10.2514/6.2018-3768
25. Cruden, B. A., and Brandis, A. M. "Measurement of Radiative Non-equilibrium for Air Shocks Between 7-9 km/s," *47th AIAA Thermophysics Conference* 2017-4535, 2017. doi: 10.2514/6.2017-4535
26. Baulch, D. L., Bowman, C. T., Cobos, C. J., Cox, R. A., Just, T., Kerr, J. A., Pilling, M. J., Stocker, D., Troe, J., Tsang, W., Walker, R. W., and Warnatz, J. "Evaluated Kinetic Data for Combustion Modeling: Supplement II," *Journal of Physical and Chemical Reference Data* Vol. 34, No. 3, 2005, pp. 757-1397. doi: 10.1063/1.1748524
27. Jesse W. Streicher, A. K., and Ronald K. Hanson. "Coupled vibration-dissociation time-histories and rate measurements in shock-heated, nondilute O2 and O2–Ar mixtures from 6000 to 14 000 K," 2021. doi: 10.1063/5.0048059
28. Schwenke, D. W., Jaffe, R. L., and Chaban, G. M. "Collisional Dissociation of CO: ab initio Potential Energy Surfaces and Quasiclassical Trajectory Rate Coefficients," *Journal of Physical Chemistry*, submitted,

29. Ebrahim, N. A., and Sandeman, R. J. "Interferometric studies of carbon dioxide dissociation in a free-piston shock tube," *The Journal of Chemical Physics* Vol. 65, No. 9, 1976, pp. 3446-3453. doi: 10.1063/1.433598
30. Tsang, W., and Herron, J. T. "Chemical Kinetic Data Base for Propellant Combustion I. Reactions Involving NO, NO2, HNO, HNO2, HCN and N2O," *Journal of Physical and Chemical Reference Data* Vol. 20, No. 4, 1991, pp. 609-663. doi: 10.1063/1.555890
31. Davies, W. O. "Carbon Dioxide Dissociation at 6000° to 11 000°K," *The Journal of Chemical Physics* Vol. 43, No. 8, 1965, pp. 2809-2818. doi: 10.1063/1.1697214
32. Park, C. *Nonequilibrium Hypersonic Aerothermodynamics*. New York: John Wiley & Sons, 1990.
33. Fairbairn, A. R. "The dissociation of carbon monoxide," *Proc. R. Soc. London A* Vol. 312, 1969, pp. 207-227
34. Fujita, K., Yamada, T., and Ishii, N. "Impact of Ablation Gas Kinetics on Hyperbolic Entry Radiative Heating," 2006. doi: 10.2514/6.2006-1185
35. Ibragimova, L. B. "Recommended rate constants of CO + O2 - reversible - CO2 + O reactions," *Khim. Fiz.* Vol. 10, 1991, pp. 307-310
36. Andersson, S., Marković, N., and Nyman, G. "Computational Studies of the Kinetics of the C + NO and O + CN Reactions," *The Journal of Physical Chemistry A* Vol. 107, No. 28, 2003, pp. 5439-5447. doi: 10.1021/jp0222604
37. Baulch, D., Cobos, C., Cox, R., Frank, P., Hayman, G., Just, T., Kerr, J., Murrells, T., Pilling, M., and Troe, J. "Evaluated kinetic data for combustion modeling. Supplement I," *Journal of Physical and Chemical Reference Data* Vol. 23, No. 6, 1994, pp. 847-848
38. Messing, I., Carrington, T., Filseth, S. V., and Sadowski, C. M. "Absolute rate constant for the CH + O reaction," *Chemical Physics Letters* Vol. 74, No. 1, 1980, pp. 56-57. doi: 10.1016/0009-2614(80)85013-5
39. P. Frank, K. A. B., and Th. Just. *21st Symp. Int Combustion*. 1988, p. 885.

Appendix A. Reference state independence

The heat flux by equation (31) is given by:

$$q_h^+ = q_c^+ + q_v^+ + \sum_s h_s r_s$$

Consider an alternative reference state basis $\bar{h}_s$, where

$$\bar{h}_s = h_s + \Delta h_{f,s} \tag{A-1}$$

The reference enthalpy shift must satisfy

$$\Delta h_{f,s} = \sum \upsilon_{sk} \Delta h_{f,k} \tag{A-2}$$

where k indexes the atoms in species s and υ_{sk} is the stoichiometry matrix as defined above. The heat flux in the new reference state is given by:

$$\bar{q}_h^+ = q_c^+ + q_v^+ + \sum_s \bar{h}_s r_s \tag{A-3}$$

The conducted and viscous fluxes do not depend on enthalpy so are unmodified by the change in basis. We now have the difference between the two heat fluxes given by:

$$\bar{q}_h^+ - q_h^+ = \sum_s (\bar{h}_s - h_s) r_s \tag{A-4}$$

Substituting the definition of the reference state shift (A-1) and the stoichiometric sum property (A-2) the difference in heat flux is now given as:

$$\bar{q}_h^+ - q_h^+ = \sum_{s,k} \upsilon_{sk} \Delta h_{f,k} r_s \quad \text{(A-5)}$$

Next we consider the fact that reactions preserve atoms:

$$\sum_s \upsilon_{sk} r_s = 0 \quad \text{(A-6)}$$

Since the summation in equation (A-5) can be taken in either order, we perform the summation over the species index *s* first, causing the right hand to go to zero and thus $q_h^+ - \bar{q}_h^+ = 0$, indicating this form of the heat flux to be independent of reference state.

Appendix B. List of chemical reactions employed in this work

In this work it was necessary to extend the Martian chemistry to include ablation products. The primary blowing products from phenolic heat shields were determined from 1D FIAT simulations to be CH_4, CO_2, CO, H_2 and H_2O. Some species that were present in lesser amounts at higher heat fluxes, such as C_3, C_2H_2 and C_2H, were not considered. A chemistry was formulated to include these species along with the typical Martian chemistries by combining works of Gokcen[22], Martin[23], Cruden[24, 25] and Baulch[26]. The 2005 review of Baulch, et al., updated several of the rates employed by Gokcen and Martin and supplied additional reaction processes which have been incorporated into the table. The newly measured rate of Streicher, et al. was substituted for O_2 dissociation[27] while the rate of CO is based upon that of Schwenke, et al., [28] but modified to account for electronic excitation as discussed in [24]. Furthermore, the CO and CO_2 dissociation rates were refit to ensure recombination rates at 300K would be consistent with reported literature. This adjustment was necessary to avoid artificial gas phase recombination in the boundary layer near a cold wall. Rates for reactions 29, 31, 34 and 40-43 were also refit from those reported in Baulch to follow the modified Arrhenius form at the relevant pressure range. A sensitivity study was performed for shocks between 3-6 km/s and allowed the elimination of NH as a species and reduced the reaction set from 77 to 39, with six less important reactions added to the table for completeness. Exothermic reactions are written in the direction reported in their original sources, as the corresponding endothermic rate is obtained in the simulation via detailed balance without loss of accuracy.

Table B-1. List of reactions included in this work

Reaction		A (cm^3/mol·s)	n	E_a (K)	Ref
1	$CO_2 + M \rightarrow CO + O + M$	1.76×10^{28}	-3.33	67,040	[29-31]
2	$CO + M \rightarrow C + O + M$	8.36×10^{35}	-4.72	129,230	[24, 28]
3	$N_2 + M \rightarrow 2N + M$	7.0×10^{21} [(a)]	-1.6	113,200	[32]
4	$O_2 + M \rightarrow O + O + M$	9.5×10^{21} [(b)]	-1.7	59,400	[27]
5	$NO + M \rightarrow N + O + M$	2.4×10^{15}	0.0	74,570	[30]
6	$C_2 + M \rightarrow C + C + M$	1.82×10^{15}	0.0	64,000	[33]
7	$CN + M \rightarrow C + N + M$	6.0×10^{15}	-0.4	71,000	[34]
8	$CH_4 + M \rightarrow CH_3 + H + M$	4.7×10^{47} [(c)]	-8.2	59,200	[26]
9	$CH_3 + M \rightarrow CH_2 + H + M$	1.02×10^{16}	0.0	45,600	[26]
10	$CH_3 + M \rightarrow CH + H_2 + M$	6.62×10^{15}	0.0	42,800	[26]
11	$CH_2 + M \rightarrow CH + H + M$	9.39×10^{15}	0.0	44,900	[26]
12	$CH_2 + M \rightarrow C + H_2 + M$	3.01×10^{14}	0.0	32,600	[26]
13	$CH + M \rightarrow C + H + M$	1.9×10^{14}	0.0	33,700	[22]
14	$H_2 + M \rightarrow H + H + M$	2.23×10^{14} [(d)]	0.0	48,400	[26]
15	$HCN + M \rightarrow CN + H + M$	3.57×10^{26}	-2.6	62,800	[22]

[(a)] Rate is increased by 4.28× when the collision partner is C, N or O
[(b)] Rate is increased by 3.5× when the collision partner is an atom, or reduced 2400× with Ar
[(c)] Rate is increased by 2× when the collision partner is CH_x
[(d)] Rate is increased by 4× when the collision partner is H or H_2

16	$H + O + M \rightarrow OH + M$ *	5.0×10^{17}	-1.0	0	[23]
17	$H + OH + M \rightarrow H_2O + M$	2.21×10^{22}	-2.0	0	[26]
18	$CH_3 + H \rightarrow CH_2 + H_2$	1.26×10^{16}	-0.56	8,000	[26]
19	$CH_2 + H \rightarrow CH + H_2$	1.2×10^{14}	0.0	0	[26]
20	$CH + C \rightarrow C_2 + H$	2.0×10^{14}	0.0	0	[22]
21	$C + H_2 \rightarrow CH + H$	4.0×10^{14}	0.0	11,700	[22]
22	$CH4 + H \rightarrow CH_3 + H_2$	6.14×10^{5}	2.5	4,830	[26]
23	$CO_2 + O \rightarrow CO + O_2$	2.71×10^{14}	0.0	33,800	[35]
24	$C_2 + O \rightarrow CO + C$	3.61×10^{14}	0.0	0	[33]
25	$CN+O \rightarrow CO+N$	2.43×10^{14}	-0.18	0	[36]
26	$CO + O \rightarrow C + O_2$	2.75×10^{14}	0.0	77,645	[28]
27	$N_2 + O \rightarrow NO + N$	1.8×10^{14}	0.0	38,249	[37]
28	$O_2 + N \rightarrow NO + O$	9.0×10^{9}	1.0	3,270	[37]
29	$CH + O \rightarrow CO + H$	1.39×10^{14}	0.0	260	[38, 39]
30	$CH_2 + O \rightarrow CO + H_2$	8.19×10^{13}	0.0	270	[26]
31	$OH + CH_3 \rightarrow CH_2 + H_2O$	2.0×10^{12}	0.0	0	[26]
32	$OH + CH_4 \rightarrow CH_3 + H_2O$	1.37×10^{6}	2.18	1,350	[26]
33	$O + CH_4 \rightarrow CH_3 + OH$	4.4×10^{5}	2.5	3,310	[26]
34	$O + H_2 \rightarrow H + OH$	5.12×10^{4}	2.67	3,170	[26]
35	$O_2 + H \rightarrow O + OH$	2.07×10^{14}	-.097	7,560	[26]
36	$OH + H_2 \rightarrow H + H_2O$	2.17×10^{8}	1.52	1,740	[26]
37	$OH + OH \rightarrow O + H_2O$	3.35×10^{4}	2.42	-970	[26]
38	$OH + C \rightarrow H + CO$	5.0×10^{13}	0.0	0	[23]
39	$OH + CH_2 \rightarrow CH + H_2O$	1.13×10^{7}	2.0	1,510	[23]
40	$OH + CO \rightarrow CO_2 + H$	3.43×10^{4}	2.14	-797	[26]
41	$O_2 + CH \rightarrow CO_2 + H$	3.0×10^{13}	0.0	427	[26]
42	$O_2 + CH \rightarrow CO + OH$	2.0×10^{13}	0.0	427	[26]
43	$O_2 + CH \rightarrow CO + H + O$	3.0×10^{13}	0.0	427	[26]
44	$CH_3 + O \rightarrow H + H_2 + CO$	1.69×10^{13}	0.0	0	[26]
45	$CH_2 + O \rightarrow CO + H + H$	1.23×10^{14}	0.0	270	[26]